A digital terrain model for a peak of (almost) eternal light close to the lunar south pole from SMART-1/AMIE images

B. Grieger[*,1]

European Space Agency (ESA), European Space Astronomy Centre (ESAC), P.O. Box 78, E-28691 Villanueva de la Cañada, Madrid, Spain

D.V. Koschny

European Space Research & Technology Centre, Keplerlaan 1, Postbus 299, 2200 AG Noordwijk, The Netherlands

Abstract

During its 18 month of science operations in lunar orbit, the Advanced Micro-Imager Experiment (AMIE) aboard the SMART-1 spacecraft acquired about 32 000 images of the lunar surface. 113 NONE filter images have captured a location close to the lunar south pole which we have identified to be a peak of (almost) eternal light. We have selected five images taken in southern lunar summer (i.e., with the sun about 1.5° above the horizon) representing diverse illumination directions to reconstruct the terrain by means of shape from shading. The approach is quite novel as it uses multiple images simultaneously by iteratively reconstructing a digital terrain model (DTM) which is consistent with the surface brightnesses observed in all images. The resultant DTM covers a square area of 20 km width with 50 m resolution.

Key words: peak of eternal light, shape from shading, digital terrain model
PACS: 96.12.Kz, 96.12.Qr, 96.20.Dt

1. Introduction

(**???**)

2. The peak of (almost) eternal light

The south polar area is considered as possible target for future lander missions. Of particular interest is the availability of sunlight on the surface over extended periods of time. Because of the low obliquity of the Moon's rotation axis, it was suspected that there may be peaks which are illuminated most of the year. Theoretically, there could even be one so-called peak of eternal light which is illuminated all the time. Because of the polar orbit of SMART-1, the polar areas could be imaged frequently. During the 18 month of science operation, images over a wide range of illumination conditions have been acquired. These allow to search for peaks with favourable lighting.

We began our search for the peak of eternal light in the south polar region by just visually browsing AMIE images. A candidate set was formed from sites which were illuminated in many images. Whenever an image was found were a candidate site was in shadow while at least one of the other candidate sites was still illuminated, the site in shadow was eliminated from
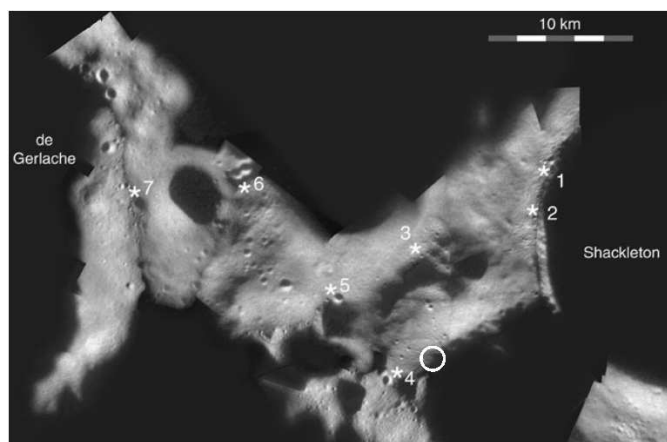

Figure 1: Mosaic of Clementine imagery. The asterisks mark landing sites under consideration for future robotic missions. The circle marks the candidate site for the peak of eternal light. Note that in this image the zero meridian is not pointing straight upward (like in the other map projected images shown herein), but slightly tiltet to the left. Mosaic with landing sites taken from **?**, by courtesy of the author.

the candidate list. This process led quickly to only one remaining candidate site for the peak of eternal light. It is located at 137°W, 17 km from the south pole, cf. Fig. **??**.

Having identified our candidate site, we inspected all AMIE NONE filter images with this site in the field of view. There are 113 such images. Their illumination conditions are illustrated in Fig. **??**. In almost all of them, that is in 109 images, the peak is illuminated, however, in four images, the peak is in shadow.

[*]Corresponding author
Email address: bjoern.grieger@esa.int (B. Grieger)
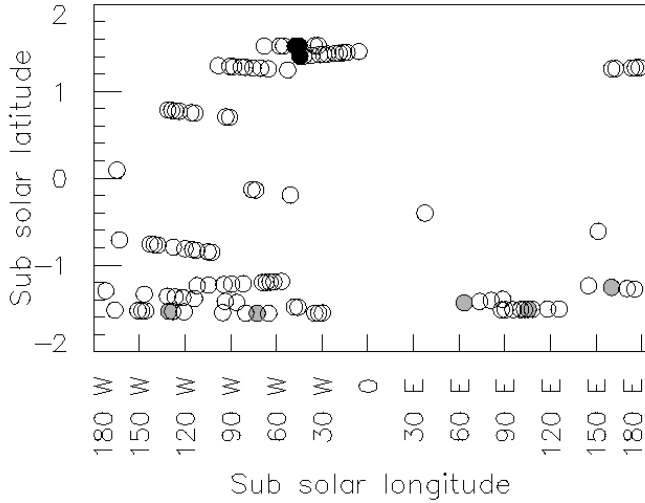[1]Telephone +34 91 81 31 107, fax +34 91 81 31 325

Figure 2: Illumination conditions for the 113 AMIE NONE filter images showing the peak of light. Note the different scale of sub solar longitude and latitude. Black filled circles represent the four images where the peak is in shadow; for the other images it is illuminated. Grey filled circles denote the five images selected for shape from shading.

The four images where the peak is dark were taken at very similar illumination conditions, with subsolar longitude close to 45°W and subsolar latitude close to 1.5°N. Thus the incidence angle is always larger than 90° when the peak is dark. This indicates that the peak may be the highest one in the area, although the light is not completely eternal.

So this site is not truely a peak of eternal light, but we could not find a better candidate. Therefore, we believe that this site is the one in the south polar area which comes closest to a peak of eternal light.

3. Images used

The selection of a set of images for a concerted shape from shading approach was driven by three conditions:

- The sun should be "high" in the sky, i.e., the sub solar latitude should be close to the lowest possbile value of −1.5°.

- The azimuths of illuminations should cover the full circle with a spacing as even as possible.

- The images should not be saturated.

The latter condition could not be perfectly met. Each of the images with acceptable illumination conditions is at least slightly saturated in some small area. Avoiding images which are heavily saturated over large areas left us with a set of five selected images. Their illumination conditions are marked by grey filled circles in Fig. **??**. The selected images are listed in Tab. **??**.

The AMIE images used herein have been dark corrected and flat fielded based on master frames created from flight data acquired in lunar orbit. All image pixels should be correctly calibrated relative to each other, however, the absolut calibration is not known.
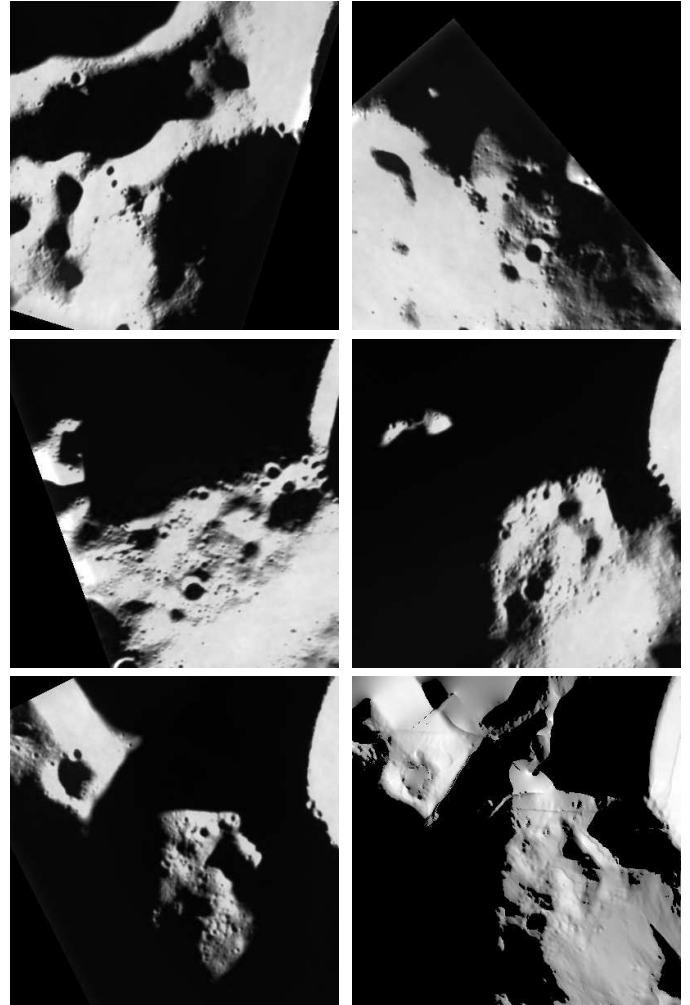

Figure 3: *Except bottom right:* The five images used for the concerted shape from shading approach, mapped to a common square grid of 20 km width in orthographic polar projection. The vertical axis is parallel to the zero meridian (north up). At the upper right margin, the wall of crater shackleton in visible. From left to right and top to bottom, the images are in the sequence of their reference numbers 1–5 as given in Tab. **??**. *Bottom right:* Model image created by rendering the reconstructed DTM, cf. Sec. **??**.

The five images are manually co-registered, which requires considerable care because of the very different illuminations. The co-registration could be done with an accuracy of 100 m, which is slightly lower than the image resolution of about 50 m per pixel. The images are then mapped to a common grid of 401×401 points with an even spacing of 50 m in orthographic polar projection. Taking the south pole as co-ordinate origin and the y-axis parallel to the zero meridian (north up), the center point of the grid is located at $x = -11$ km, $y = -12$ km. The five mapped images are shown in Fig. **??**.

4. Multi-illumination shape from shading

4.1. Approach and grid layout

Combining several images does not only provide more illuminated area but does also much better constrain the generally ill-posed shape from shading problem. Let i and e be incidence

Ref	Orb#	Img#	D [AU]	Inc [°]	Em [°]	SLon [°]	SLat [°]	Δx [km]	Δy [km]
1	1667	3	0.9846	88.19	1.40	−72.60	−1.55	0.0	0.0
2	1690	3	0.9820	87.91	0.96	−130.66	−1.53	0.0	−0.3
3	1860	3	0.9830	88.51	0.97	160.15	−1.23	−0.9	0.1
4	1739	3	0.9829	88.77	0.83	105.45	−1.51	−0.5	0.0
5	1613	1	0.9860	89.10	1.44	63.41	−1.43	−0.2	−0.2

Table 1: List of the five selected images. The columns provide a reference number used herein, the orbit number, the image number (in this orbit), the distance of the Moon from the Sun, incidence angle, emision angle, sub solar longitude, sub solar latitude, and the translations applied in x and y direction to coregister the images.
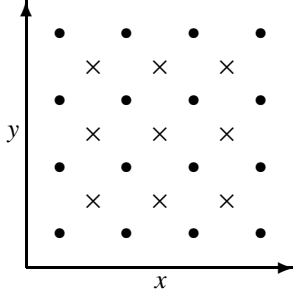

Figure 4: Points of the DTM elevation grid (•) and points of the grid of brightnesses and slope constraints (×). The actual brightness grid has 401×401 points, the actual DTM grid has 402×402 points.

and emmission angle, respectively. Assuming the Lommel-Seeliger law, the surface reflectance function is

$$r_{LS} \propto \frac{\cos i}{\cos i + \cos e}. \qquad (1)$$

The observed surface brightness does only depend on the slope in the downsun direction (on photometric longitude), but *not* crosswise to it (on photometric latitude). Therefore, from a single image, one can only compute profiles in the downsun direction, but the elevation of these profiles relative to each other is unknown. With our approach combining information from different illumination directions, we directly compute a full 3D Digital Terrain Model (DTM), not just profiles. Starting out from a flat surface, the elevation values of the grid points of the DTM are iteratively adjusted to yield slopes between these points which are compatible with the observed brightnesses in *all* images.

We define the grid of elevation points for the DTM in a way which puts the points of observed brightnesses just in between the DTM points, as the brightnesses constrain the slopes between these points, cf. Fig. **??**. In climate modelling, this type of staggered grids representing scalar and gradient related quantities is known as Arakawa B grid.

4.2. Initial computations

Our evenly spaced grids are defined in orthographic polar projection, with the y-axis parallel to the zero meridian (north up), cf. Fig. **??**. For each image $k = 1 \ldots 5$, the downsun direction measured counterclockwise from the x-axis is

$$\phi_{\odot}(k) = -(\text{SLon}(k) + 90°), \qquad (2)$$

where SLon is the sub solar longitude, cf. Tab. **??**. Each (inner) DTM pixel has four diagonal neighbours: bottom left (bl),

bottom right (br), top right (tr) and top left (tl). Any constraint on the slope to a neighbouring pixel is only strong if the pixel lies in the downsun (or upsun) direction of the image which imposes the constrain (cf. Sec. **??**). Therefore, for each image, we introduce weighting factors depending on the cosine beween the direction to the diagonal neighbour pixel and the downsun direction:

$$\mu_{\text{bl}}(k) = \cos(\phi_{\odot}(k) - 45°), \qquad (3)$$
$$\mu_{\text{br}}(k) = \cos(\phi_{\odot}(k) - 135°), \qquad (4)$$
$$\mu_{\text{tr}}(k) = \cos(\phi_{\odot}(k) - 225°), \qquad (5)$$
$$\mu_{\text{tl}}(k) = \cos(\phi_{\odot}(k) - 315°). \qquad (6)$$

Throughout our computations, we make the approximative assumption that the camera looked exactly vertically down onto our grid. This is correct within less than two degrees concerning the very small nominal (flat surface) emission angles (cf. Tab. **??**) and the proximity of the target area to the south pole. With this assumption, the phase angles of the images $k = 1 \ldots 5$ are simply

$$\alpha(k) = 90° + \text{SLat}(k), \qquad (7)$$

where SLat is the sub solar latitude, cf. Tab. **??**.

Let the observed brightnesses from the images be given by

$$\left(B(k, i_x, i_y)\right)_{k=1\ldots5,\ i_x=1\ldots401,\ i_y=1\ldots401}, \qquad (8)$$

with k denoting the image and i_x, i_y numbering the pixels. If an image does not cover the complete grid, the uncovered pixels are marked invalid. In addition, shadow pixels are marked invalid. We consider a pixel to be in shadow if $B(k, i_x, i_y) < 0.1$. The threshold value of 0.1 has been chosen in order to reproduce the shadow assessment of the human eye. No unit can be given for the AMIE brighness values, because they have not yet been absolutely calibrated.

We have to prescribe a *brightness scaling factor A*. This factor comprises the surface albedo (which is assumed to be constant) and the unkown absolute calibration of the camera. The factor A is adjusted by a trial and error procedure as described in Sec. **??**. The finally adopted value is

$$A = 8. \qquad (9)$$

Following the Lommel-Seeliger law (cf. Sec. **??**), we define a normalized surface reflectance function in dependence on phase angle α and emmission angle e, i.e.

$$R(\alpha, e) = \begin{cases} \frac{\cos i}{\cos i + \cos e} & \text{if } \cos i > 0 \text{ and } \cos e > 0, \\ 0 & \text{else,} \end{cases} \qquad (10)$$

3

where the incidence angle is simply

$$i = e - \alpha, \tag{11}$$

because we assume that the surface slope has only a downsun component. Based on this, we also define the inverse function which computes the emmission angle in dependence on phase angle α and normalized brightness b, i.e.

$$E(\alpha, b) = \left| \arccos \left(\frac{\sin \alpha}{\sqrt{\left(\frac{b}{1-b} - \cos \alpha \right)^2 + \sin^2 \alpha}} \right) \right| \cdot$$
$$\cdot \operatorname{sign}(b - R(\alpha, 0)). \tag{12}$$

With the help of these function, we can compute for each pixel (i_x, i_y) of each image k the step in elevation between two diagonally neighboured DTM grid points which would be required to reproduce the observed brightness (if the DTM grid point separation was in downsun direction):

$$s(k, i_x, i_y) = \sqrt{2}\, d \cdot \tan \left(E \left(\alpha_k, \min \left(1, \frac{B(k, i_x, i_y)}{A} \right) \right) \right), \tag{13}$$

where $d = 50$ m is the grid spacing. Theoretically, $B(k, i_x, i_y)/A$ should not be larger than unity, however, because of an (initially) improper choice of the brightness scaling factor A and because of measurement errors, it might happen, and therefore we constrain the argument of E. The elevation step s in only computed for valid pixels, i.e., for pixels for which a brightness measurement is available *and* which are not in shadow.

The elevations of the DTM are defined on a 402×402 grid which is staggered with the grid of brightnesses and elevation steps as illustrated in Fig. **??**. Let the elevations be given by

$$\left(z(i_x, i_y) \right)_{i_x = 0 \ldots 401,\ i_y = 0 \ldots 401}. \tag{14}$$

Note that the grid point indexing starts with 0 for z, while it starts with 1 for B and s. The slope point $s(k, 1, 1)$ lies in the center beween the diagonal neighbours $z(0, 0)$ and $z(1, 1)$ (and also between $z(1, 0)$ and $z(0, 1)$). The elevations $z(i_x, i_y)$ are initiallized with zero.

4.3. Iterative computation of the DTM

In each iteration step, a new value for the elevation of each grid point is computed according to

$$z'(i_x, i_y) = \frac{\sum_{k=1}^{5} \sum_{j=1}^{4} w_{kj} \xi_{kj} + \sum_{i=1}^{4} \lambda \zeta_i}{\sum_{k=1}^{5} \sum_{j=1}^{4} w_{kj} + 4\lambda}. \tag{15}$$

Here w_{kj} and λ are weighting factors and ξ and ζ are elevations imposed by certain conditions. The index k runs over all images, j runs over all diagonal neighbours of the DTM pixel (i_x, i_y), and i runs over all orthogonal neighbours.

The old elevation of the bottom left neighbour is $z(i_x - 1, i_y - 1)$. To reproduce the observed brightness $B(k, i_x, i_y)$, the elevation at (i_x, i_y) should be

$$\xi_{k1} = z(i_x - 1, i_y - 1) + s(k, i_x, i_y) \cdot \mu_{\mathrm{bl}}(k), \tag{16}$$

cf. Eqs. (**??**, **??**). The weighting factor for this contribution is

$$w_{k1} = \mu_{\mathrm{bl}}(k)^2, \tag{17}$$

which gives unity if the two DTM points are separated parallel to the downsun direction and zero if the separation is orthogonal. The contributions of the other three diagonal neighbours are

$$\xi_{k2} = z(i_x + 1, i_y - 1) + s(k, i_x + 1, i_y) \cdot \mu_{\mathrm{br}}(k), \tag{18}$$
$$\xi_{k3} = z(i_x + 1, i_y + 1) + s(k, i_x + 1, i_y + 1) \cdot \mu_{\mathrm{tr}}(k), \tag{19}$$
$$\xi_{k3} = z(i_x - 1, i_y + 1) + s(k, i_x, i_y + 1) \cdot \mu_{\mathrm{tl}}(k), \tag{20}$$

with the weighting factors

$$w_{k2} = \mu_{\mathrm{br}}(k)^2, \tag{21}$$
$$w_{k3} = \mu_{\mathrm{tr}}(k)^2, \tag{22}$$
$$w_{k4} = \mu_{\mathrm{tl}}(k)^2. \tag{23}$$

Each contribution is only computed and applied if there actually is a neighbour DTM point within the grid boundaries *and* if the brightness grid point halfway to the DTM point is valid.

The orthogonal DTM neighbour points are used to provide smoothness constraints. Their contribution is simply

$$\zeta_1 = z(i_x - 1, i_y), \tag{24}$$
$$\zeta_2 = z(i_x + 1, i_y), \tag{25}$$
$$\zeta_3 = z(i_x, i_y - 1), \tag{26}$$
$$\zeta_4 = z(i_x, i_y + 1). \tag{27}$$

The respective weighting factor, cf. Eq. (**??**) is set to

$$\lambda = 0.005. \tag{28}$$

Because this value is usually small compared to the weighting factors w_{kj}, the smoothness contraints only take effect when no valid neighbouring brightness points are available or when all valid brightness neighbours lay almost crosswise to the downsun direction. The smoothness contributions do not depend on valid brightness points, thus they are computed for all orthogonal neighbours (as long as they are within the grid boundaries). The (albeit weak) constraint of smoothmess between orthogonal neighbours also prevents the separation into two subgrids, a well known problem of the Arakawa B grid if only interaction between diaogonal neighbours is concidered.

At the end of each iteration, the grid of new elevations $z'(i_x, i_y)$ is copied to the old elevations $z(i_x, i_y)$. We apply 100 000 such iterations. After this, the change by each iteration has decreased to almost zero.

4.4. Adjustment of the brightness scaling factor

As stated in Sec. **??**, we have to prescibe a brightness scaling factor, cf. Eq. (**??**). This scaling factor A is a priori unknown. It is important to note that for grazing incidence — i.e., incidence angles close to 90° — the brightness is approximately linearly related to (the downsun component of) surface slope. This holds for the Lommel-Seeliger reflectance functino as well as for other common reflectance functions. The propotionality

4

constant of this linear relation varies between relectance functions, but it can be incorporated in our brightness scaling factor. Therefore, our DTM reconstruction does *not* depend very much on the actual choice of the relectance function.

However, the reconstruction depends on the scaling factor. Because of the approximately linear relations between surface slope and brightness, the elevations of the resultant DTM scale (inversely) with the assumed brightness scaling factor A. To constrain the DTM, we use the extent of shadows. Shadows are not used in the actual DTM reconstruction. We just ignore shadowed areas and concider only local surface slope. Taking into account the obscuration of the sun by distant terrain would be much too expensive computationally to be incorporated in the shape from shading procedure. However, if a DTM is given, it is possible to render it concidering local surface slope *and* shadows casted by distant terrain. For our purpose, it is sufficient to treat interreflection only approcimatively as described by ???.

Therefore, we adopt the following procedure to constrain the brightness scaling factor:

1. Start with an initial guess for the scaling factor A.
2. Compute a DTM by means of multi-illumination shape from shading.
3. Render the DTM, tracing shadows casted by distant terrain.
4. Compare the rendered image to the observed image.
5. If the rendered image shows too much shadow, increase A; if it shows too little shadow, decrease A.
6. Repeat from 2. until the extent of shadow matches.

For comparison, we use the image with reference number 5, cf. Tab. **??**. To the bottom right of Fig. **??**, the model image created by rendering the final DTM with the illumination condition of image 5 is shown, side by side with the real image 5. While at first sight there seem to be significant discrepancies, the similarity is in fact quite satisfactory. The differences near the top edge of the image are in an area which is partly dark in all images and partly only illuminated in one image (number 1), thus the DTM is not very well contrained in this area (cf. also Sec. **??**). The differences in the lower right are caused by shadows casted by terrain outside the DTM domain, thus they can not be reproduced by just rendering the DTM. The correct height scaling of the DTM is confirmed by the reproduced extent of shadow casted by the rim of Shackleton crater onto the flank of the peak (close to center of right edge) and onto the flank of of the elevated crater at the top left (straight diagonal shadow line).

5. Results and discussion

The resultant DTM is illustrated in Figs. **??** and **??**.

Fig. **??** shows an oblique view of the DTM which was created by projecting image 5 onto the DTM.

Particularly for the planning of future lander missions, the retrieved DTM is of great interest. It has also been used for outreach purposes by producing a movie of a simulated fly over.
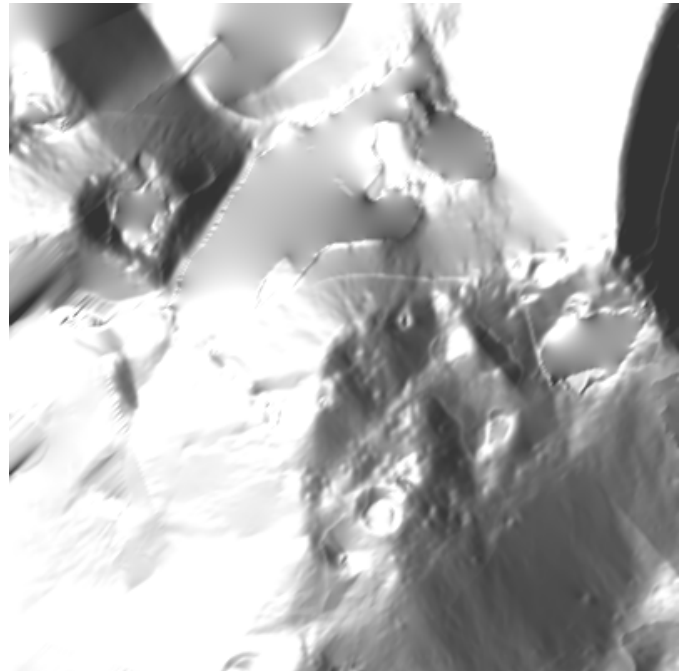

Figure 5: DTM rendered with simple realtime 3D renderer and artificial lighting for illustration. The DTM consists of 402×402 grid points with 50 m spacing. For the actual elevation in meters see Fig. **??**.
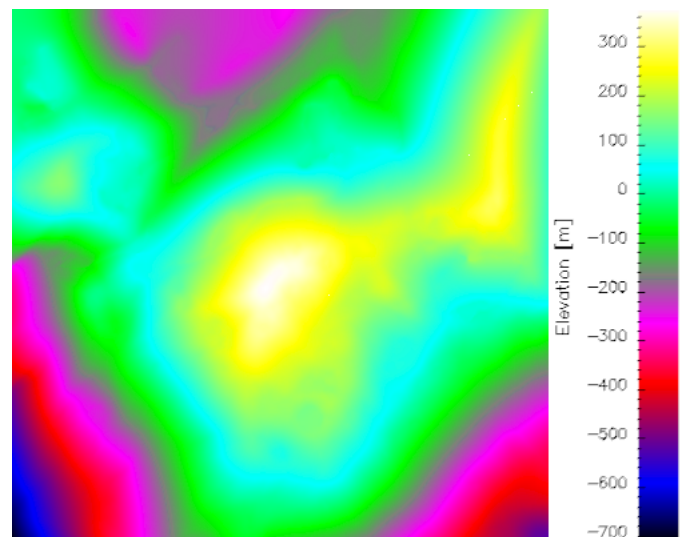

Figure 6: DTM elevation (color in the online version). The zero level is arbitrary.

Figure 7: Oblique view of the peak of (almost) eternal light, created by projecting image 5 onto the DTM. The elevation is exaggerated five times. In the foreground is the inner crater wall of Shackleton.